Engineering xxx (xxxx) xxx

Contents lists available at ScienceDirect

Engineering

journal homepage: www.elsevier.com/locate/eng

Research
Agricultural Engineering—Article

Revealing the Native Multi-Enzyme Synergy of *Acinetobacter calcoaceticus* SDH15 for Ultra-Long-Chain Alkane Biodegradation

Xianrui Liu [a], Donghuan Su [a], Shaojie Wang [a], Zhenxia Du [b], Haijia Su [a,*]

[a] *State Key Laboratory of Green Biomanufacturing, Beijing Key Laboratory of Green Chemicals Biomanufacturing, National Energy R&D Center for Biorefinery, Beijing Synthetic Biomanufacturing Technology Innovation Center, Beijing University of Chemical Technology, Beijing 100029, China*
[b] *College of Chemistry, Beijing University of Chemical Technology, Beijing 100029, China*

ARTICLE INFO

Article history:
Received 13 November 2025
Revised 3 February 2026
Accepted 10 February 2026
Available online xxxx

Keywords:
Long-chain alkane
Polyethylene
Multi-enzyme synergy
Genomics
Transcriptomics

ABSTRACT

Polyethylene (PE) biodegradation is critical, yet microbial degradation of its ultra-long-chain alkane (ULCA, > C22) components remains limited and poorly understood beyond C40. This study identified *Acinetobacter calcoaceticus* (*A. calcoaceticus*) SDH15, a novel strain capable of degrading solid *n*-alkanes up to C56, thereby significantly extending the known biological range of alkane catabolism. Integrated genomic and transcriptomic analyses revealed a four-module enzymatic system driving this process. The first module, chemotaxis and adsorption, employs an upregulated PilH-Chp chemosensory system and type IV fimbriae (T4P), with *fimF/G* expression increased up to 332-fold, for substrate sensing and attachment. The second module, transmembrane transport, involves upregulated genes encoding outer membrane proteins (*fadL*, *ompW*, and *tonB*) and inner membrane transporters (*mfs*/*emrAB-tolC*; up to 18.9-fold) that facilitate alkane uptake. The third module, oxidative degradation, is initiated by the AlkB-type alkane monooxygenase AlkMa, which is encoded by the dramatically upregulated *alkMa* gene (327.7-fold for C22) and is essential for ULCAs oxidation, followed by alcohol and aldehyde dehydrogenases (ALDHs). The fourth module, energy metabolism, couples β-oxidation with an adaptive glyoxylate cycle to conserve carbon. Furthermore, electrospray ionization mass spectrometry enabled direct detection of C56 fatty acid intermediates, providing molecular evidence of the pathway's broad substrate capacity. Functional validation through *alkMa* gene deletion confirmed its indispensable role in the initial oxidation of C22–C30 alkanes. This study presents a comprehensive model of native multi-enzyme synergy underlying ULCAs biodegradation, offering a framework for engineering microbial systems for PE remediation.

1. Introduction

Polyethylene (PE), the most widely produced plastic globally, poses a persistent and increasing environmental threat due to the extreme recalcitrance of its carbon–carbon backbone [1]. While conventional physicochemical recycling methods are often energy-intensive and environmentally detrimental [2,3], microbial biodegradation offers a scalable and sustainable alternative [4,5]. However, the development of effective biocatalytic solutions is fundamentally limited by our incomplete understanding of how microorganisms overcome the chemical inertia of PE's structure. To address this challenge, paraffin and polyethylene (PE) wax are frequently employed as ideal structural models [6,7]. These materials, comprised of ultra-long-chain alkanes (ULCAs, > C22), mimic the fundamental carbon–carbon backbone of PE [8]. While not capturing the high polymerization degree of PE, they enable a detailed investigation of the enzymatic mechanisms required for the initial oxidation of such highly hydrophobic and solid substrates.

Despite this strategic approach, two critical barriers impede progress. The first barrier is the apparent biological limit of alkane catabolism. While many microorganisms can metabolize medium- and long-chain alkanes, efficient degradation rarely exceeds C40 [9]. For instance, *Acinetobacter* sp. DSM17874 has been shown to utilize *n*-alkanes up to C40 [10]. Furthermore, only a few specialized isolates, such as *Acinetobacter* sp. M-1 and a microorganism described simply as a "short gram-negative rod" due to the

* Corresponding author.
E-mail address: suhj@mail.buct.edu.cn (H. Su).

https://doi.org/10.1016/j.eng.2026.02.035

Please cite this article as: X. Liu, D. Su, S. Wang et al., Revealing the Native Multi-Enzyme Synergy of *Acinetobacter calcoaceticus* SDH15 for Ultra-Long-Chain Alkane Biodegradation, Engineering, https://doi.org/10.1016/j.eng.2026.02.035

taxonomic limitations of the era, exhibit a limited capacity to degrade C44 [11,12]. Consequently, the C40–C44 range has largely been considered the practical recalcitrance threshold, beyond which degradation by most microorganisms becomes negligible or undetectable. This "carbon chain ceiling" suggests that initiating the breakdown of ULCAs, which is the crucial first step in PE oligomer degradation, requires a highly specialized enzymatic mechanism that remains largely uncharacterized.

The second barrier is analytical, specifically hindering our ability to trace the metabolic pathway. Conventional studies on PE biodegradation often rely on gas chromatography–mass spectrometry (GC–MS) to analyze final products, which are typically heterogeneous mixtures of low-molecular-weight compounds [13–15]. Such analyses confirm degradation but offer limited insight into the specific enzymatic steps of the initial depolymerization cascade. For ULCAs, the canonical terminal oxidation pathway proceeds through long-chain fatty alcohols and fatty acids [16]. However, long-chain fatty alcohols are challenging to detect and quantify due to their chemical properties and low abundance, rendering them unsuitable as primary metabolic markers. Consequently, their corresponding ultra-long-chain fatty acids (ULCFAs) emerge as the most direct and reliable intermediates for elucidating the degradation pathway [17,18]. However, even these ULCFAs, particularly those exceeding C30, present a major challenge for traditional GC–MS, which struggles with their low volatility and thermal instability [19]. This creates a critical analytical void in understanding ULCAs metabolism.

Microbial alkane degradation relies on a sophisticated, multi-enzyme system. The process typically initiates with by terminal oxidation, where alkane monooxygenases catalyze the initial hydroxylation. Subsequent oxidation by alcohol and aldehyde dehydrogenases (ALDHs) converts the alkane into a fatty acid, which is then catabolized through the β-oxidation pathway [20]. Key enzymatic modules for these steps have been identified in various model organisms. For instance, diverse AlkB-type non-heme integral membrane monooxygenases have been characterized in species such as *Acinetobacter venetianus* (*A. venetianus*) RAG-1 [21,22], and *Acinetobacter oleivorans* (*A. oleivorans*) DR1 [23]. These demonstrate a broad capacity to initiate alkane breakdown. Other enzymes, such as the soluble LadA-type monooxygenase in *Geobacillus thermodenitrificans* NG80-2, were also proposed to have this function [24], although recent biochemical evidence has challenged this role [25]. This highlights the importance of identifying the primary catalysts in specific organisms. Furthermore, alternative pathways exist, exemplified by the recently reclassified AlmA, a Baeyer–Villiger monooxygenase involved in sub-terminal oxidation pathways [26]. While these and other omics-based studies in bacteria such as *Alcanivorax dieselolei* (*A. dieselolei*) [27], *A. venetianus* [28,29], and *Dietzia* sp. [30] have successfully pinpointed crucial enzymes and pathways for medium- to long-chain alkanes, their focus has largely remained on individual functional modules or components operating below the C40 threshold. Consequently, there is a notable lack of a systemic and integrated understanding of how microbes coordinate the entire degradation cascade, from substrate sensing and uptake to initial oxidation and central metabolism, particularly with regard to solid ULCAs. This critical knowledge gap regarding native multi-enzyme synergy fundamentally limits our ability to rationally design synthetic microbes capable of degrading PE oligomer, a necessary component of a complete bioremediation solution.

Here, we directly address these challenges by discovering and comprehensively characterizing *Acinetobacter calcoaceticus* (*A. calcoaceticus*) SDH15. This novel soil isolate that dramatically expands the known frontier of microbial catabolism by mineralizing solid *n*-alkanes up to C56. Employing an integrated multi-omics and genetic approach, we decipher the molecular mechanism of the native multi-enzyme synergy. We reveal a highly coordinated four-module system governing substrate capture, transmembrane transport, oxidative degradation, and adaptive energy metabolism. In addition, we overcome the analytical bottleneck by strategically targeting ULCFA intermediates and developing an electrospray ionization mass spectrometry (ESI–MS) method to provide the first direct molecular evidence of intermediates as large as C56 acid. By elucidating this comprehensive model of native enzyme coordination, our study not only provides a foundational understanding of ULCAs catabolism but also offers a blueprint for the rational engineering of synthetic biological systems aimed at mineralizing PE waste.

2. Materials and methods

2.1. Bacterial strains, chemicals, and culture conditions

A. calcoaceticus SDH15 was isolated from landfill soil. All bacterial strains, plasmids, and primers used in this study are listed in Tables S1 and S2 in Appendix A. Strains were routinely cultured in Luria–Bertani (LB) medium or minimal salts medium (MSM) at 37 °C with 200 r•min^{-1} [31]. All liquid cultures were performed in 100 mL Erlenmeyer flasks, covered with breathable sealing film to ensure adequate aeration. All *n*-alkanes and other major chemicals were purchased from Macklin (China). A detailed protocol is provided in the Methods S1 and S2 in Appendix A.

2.2. Degradation of long-chain n-alkanes (C22–C40), liquid paraffin, and PE wax

For all assays, strain SDH15 was pre-cultured in LB, harvested (6000 r•min^{-1}, 5 min), washed twice, and resuspended in MSM. Washed cells were inoculated into 10 mL MSM (initial OD_{600} = 0.05) containing the indicated hydrocarbon as the sole carbon source. Individual solid *n*-alkanes (C22, C26, C30, C32, C34, C36, C38, C40) were pre-weighed, sterilized by ultraviolet radiation (UV) irradiation for 20 min in a laminar flow hood, and added at 0.05% (w/v). Light and heavy liquid paraffins were each added directly at 0.1% (w/v). PE wax was prepared in the same manner as the solid *n*-alkanes and added at 0.2% (w/v). Strain SDH15 was incubated for 5 days in *n*-alkanes and liquid paraffin, and for 25 days in PE wax. All conditions are subjected to three biological replicates (n = 3).

2.3. Analysis of long-chain alkanes, liquid paraffin, and PE wax

2.3.1. Quantification of residual hydrocarbons

Residual long-chain alkanes were extracted with an equal volume of *n*-hexane, concentrated by nitrogen blowdown, and then by redissolution in 1 mL *n*-hexane. The degradation efficiency of long-chain alkanes was detected by gas chromatography (GC-2014c; Shimadzu, Japan) equipped with an HP-5 (30 m × 320 μm × 0.25 μm) column and nitrogen as the carrier gas [21]. The degradation efficiency was calculated using the formula: 100% × [(initial concentration − residual concentration)/initial concentration]. The GC temperature program was provided in the Methods S3 in Appendix A. All experiments were conducted in at three biological replicates (n = 3). Data are presented as mean ± standard deviation.

2.3.2. Fatty acid extraction and analysis

Following the incubation period, the entire 10 mL culture mixture (including cells, residual substrate, and medium) was subjected to cell disruption to ensure a comprehensive extraction of all metabolic intermediates. Products were extracted using a

dichloromethane: methanol (2:1, v/v) protocol based on the Folch method [32] and analyzed by ESI–MS. Detailed extraction procedures and ESI–MS parameters are provided in the Methods S4 in Appendix A.

2.3.3. High-temperature gel permeation chromatography (HT-GPC) analysis

Molecular weight distributions of PE wax were determined by HT-GPC following the procedure by Liu et al [31]. In brief, 1,2,4-trichlorobenzene was used as the mobile phase at a flow rate of 1.0 mL·min^{-1} and a column temperature of 150 °C. The difference was that the detection was optimized using 2× PLgel MIXED-B LS, 300 mm × 7.5 mm columns.

2.4. Emulsification activity and cell surface hydrophobicity

Emulsification activity was determined using the method described by Liu et al. [33], with minor modifications. Bacterial adhesion to hydrocarbons (BATH) was measured as described by Rosenberg et al. [34]. Detailed procedures are provided in the Methods S5 in Appendix A.

2.5. Transmission electron microscopy (TEM)

Strain SDH15 cells, grown on C22 or sodium acetate for 3 days, were fixed in 2.5% glutaraldehyde, post-fixed in 1% osmium tetroxide, dehydrated with an ethanol gradient, and embedded prior to imaging on a Hitachi HT7800 TEM at 80 kV. A detailed protocol is provided in the Methods S6 in Appendix A.

2.6. Genetic manipulations and functional validation

To investigate the function of the primary oxidase, a deletion mutant of *alkMa* (SDH15Δ*alkMa*) was constructed via two-step homologous recombination [29], and its physiological role was assessed by comparing its growth and degradation performance to the wild-type. For the downstream dehydrogenases, candidate genes (*adh* and *aldh*) were heterologously expressed in *Escherichia coli* (*E. coli*) BL21(DE3), and their specific catalytic functions were validated using whole-cell biocatalysis assays. Detailed protocols for all procedures are provided in the Methods S7 and S8 in Appendix A.

2.7. Genome sequencing and transcriptome analysis

Whole-genome sequencing of strain SDH15 was conducted using the Illumina PE150 platform and the PacBio Sequel system, followed by genome assembly, annotation, and phylogenetic classification. Transcriptome sequencing was conducted on cells grown in MSM with C22, C30, or sodium acetate (each at 2 g·L^{-1}) as the sole carbon source (three biological replicates). Differential expression was evaluated using DESeq2, with a significance threshold set at an adjusted *P*-value (padj) < 0.05 and |log2(fold change)| > 1. Detailed methodologies, including library preparation, software versions, parameters, analytical pipelines, and data visualization, are provided in the Materials S9 and S10 in Appendix A.

3. Results and discussion

3.1. Isolation and genomic characteristics of alkane-degrading strain SDH15

To identify microorganisms capable of degrading ULCAs, bacteria were isolated from soil collected at a landfill enriched with PE plastic waste. Among the 91 isolates, strain SDH15 demonstrated exceptional growth when solid long-chain alkanes were provided as the sole carbon source (Fig. S1 in Appendix A). Phylogenetic analysis of the 16S ribosomal RNA (rRNA) gene revealed that strain SDH15 belongs to *A. calcoaceticus*, sharing 99.8% sequence similarity with its closest species (Fig. S2 in Appendix A).

Whole-genome sequencing was performed to precisely determine its taxonomic position and elucidate the genetic basis of alkane metabolism. The complete genome of strain SDH15 consists of a circular chromosome approximately 4.0 Mb (GC content: 38.79%) and two plasmids (Fig. S3 in Appendix A). Phylogenetic analysis of the strain SDH15 genome revealed its distinct taxonomic position among alkane-degrading strains (Fig. 1). The average nucleotide identity between strain SDH15 and the reference *A. calcoaceticus* genome (RS_GCF_000368965.1) was 96.34%. Genome-wide annotation revealed comprehensive alkane degradation genes, including alkane transporters, alkane oxidases, alcohol dehydrogenase (ADH), and ALDH. Strain SDH15 contains multiple alkane oxidase genes, such as *alk*, *almA*, and *ladA* (Table 1 [22,23,26,27,29,35,36]), which contribute to degradation through different alkane hydroxylase systems. The abundant enzyme system indicates the metabolic diversity of strain SDH15 and its potential for oxidizing various alkanes.

3.2. Broad-spectrum alkane degradation by strain SDH15

The alkane degradation potential of strain SDH15 was systematically evaluated using solid ULCAs as substrates. Strain SDH15 exhibited growth on alkanes ranging from C22 to C40 (Fig. 2(a) and Fig. S4 in Appendix A). Growth was most pronounced on C22 and C26, and while it gradually declined for longer-chain substrates (C30–C40), it remained significantly higher than the alkane-lacking control, confirming its ability to metabolize ULCAs. Strain SDH15 also demonstrated degradation of complex hydrocarbon mixtures, including light (C10–C24) and heavy (C10–C40) liquid paraffins (Figs. S5(a) and (b)). Gas chromatography analysis revealed effective utilization of mixture components, with a distinct preference for shorter-chain alkanes. This preference is likely due to a combination of factors: the higher bioavailability of shorter, liquid alkanes compared to their solid, longer-chain counterparts, and the potential substrate specificities of the various alkane hydroxylases present in strain SDH15 [37,38].

To determine the upper limit of its degradation range, further experiments on the degradation of PE wax by strain SDH15 were conducted. PE wax is an ideal PE model, containing ULCAs. After 25 days of cultivation, HT-GPC showed a significant change in the molecular weight distribution of PE wax. Alkanes with molecular weights lower than C56 (calculated as 795/14 ≈ 56.7; C55H112, M_w = 772; C57H116, M_w = 800) were degraded (Fig. 2(b)). Specifically, the lower-molecular-weight fraction of the control wax was preferentially degraded by strain SDH15. This consumption resulted in the apparent peak of the residual material shifting to ~795 Da, establishing this molecular weight as the approximate upper limit of degradation. These findings significantly expanded the known microbial alkane degradation limit, surpassing the previously reported threshold of approximately C40 [9].

3.3. Intermediate products of long-chain alkane metabolism

To elucidate the metabolic pathway of ULCAs degradation by strain SDH15, we focused on identifying key metabolic intermediates. The terminal oxidation pathway typically generates long-chain fatty alcohols, which are subsequently oxidized to fatty acids. Given the significant analytical challenges in detecting long-chain fatty alcohols, we strategically targeted the more stable and informative ULCFAs as direct evidence of this oxidative

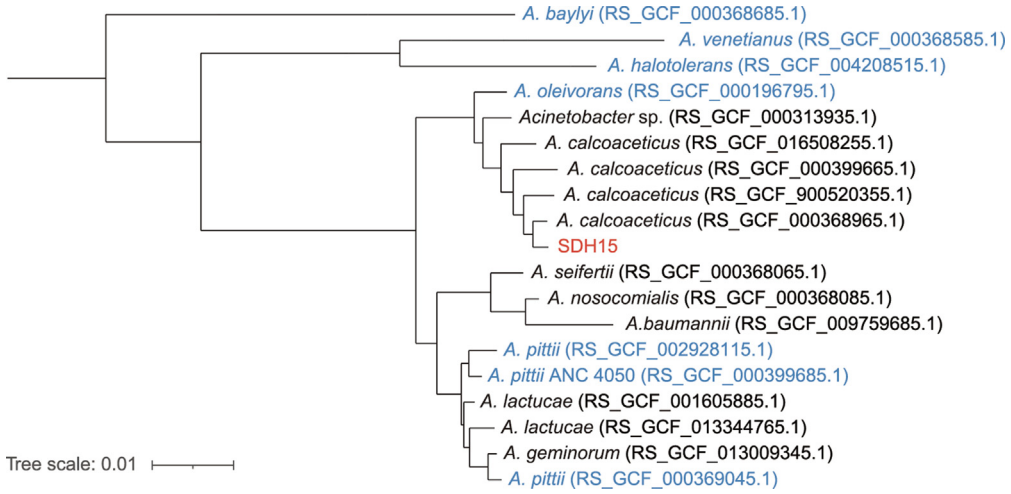

Fig. 1. Phylogenetic tree of strain SDH15. The tree was constructed using reference genomes from the genome taxonomy database (GTDB) and visualized with iTOL software. Strain SDH15 is highlighted in red, while literature-reported alkane-degrading bacteria are shown in blue.

Table 1
Homologous comparison of enzymes related to alkane degradation as reported in the literature.

Function	Enzymes	Substrates	Protein ID	Identities	Reference
Transporter	AltL (ACL9Z5_3133)	C20–C38 alkane	WP_171054784	83.2%	[29]
Alkane oxidation	AlkMa (ACL9Z5_2022)	C24–C26 alkane	WP_013198046.1	98.5%	[23]
Alkane oxidation	AlkMb (ACL9Z5_2611)	C12–C16 alkane	WP_013198473.1	96.5%	[23]
Alkane oxidation	AlmA (ACL9Z5_437)	C10–C16 aliphatic 2-ketones	WP_004924170.1	79.3%	[26]
Alkane oxidation	AlmA (ACL9Z5_437)	C10–C36 alkane	AFT70326.1	51.5%	[27]
Alkane oxidation	LadA (ACL9Z5_2210)	C15–C36 alkane	ABO68832	50.8%	[35]
ADH	ADH (ACL9Z5_1424)	C1–C32 alcohol	WP_004879683.1	92.8%	[22]
ALDH	ALDH (ACL9Z5_1421)	C1–C14 aldehyde	Q9FDS1	88.3%	[36]

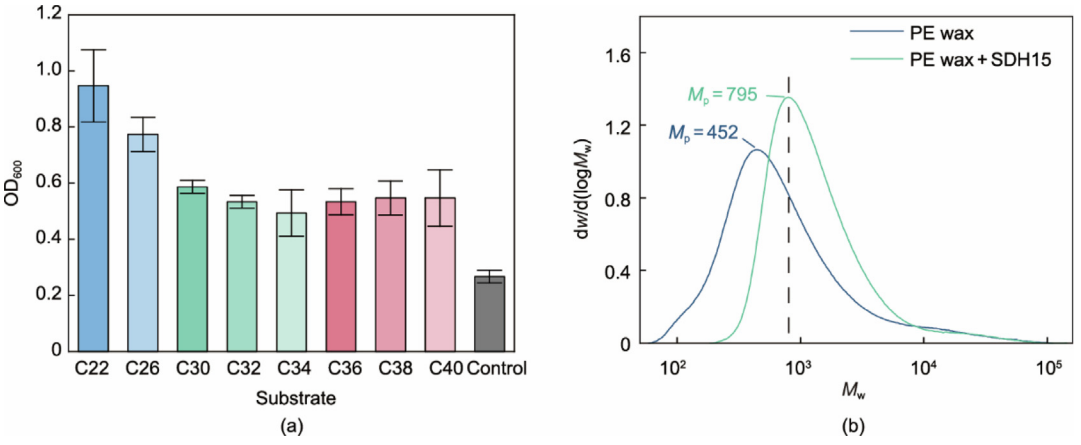

Fig. 2. Broad-spectrum alkane degradation capability of strain SDH15. (a) OD_{600} of strain SDH15 after 5 days of growth on C22–C40 alkanes. The control consists of strain SDH15 without a carbon source. (b) HT-GPC curves of PE wax degraded by strain SDH15 after 25 days. *M*: molecular weight; M_p: peak molecular weight; *w*: weight fraction.

cascade. Traditional GC–MS methods are inadequate for analyzing ULCFAs beyond C30 due to their low volatility. Therefore, this study employed ESI–MS, a technique well-suited for analyzing large, non-volatile molecules, to detect these key intermediates directly [17,39]. The method was calibrated and validated using C22, C26, and C30 fatty acid standards, confirming its reliability for subsequent analyses (Figs. 3(a)–(c)).

In degradation assays with *n*-alkanes, the corresponding C22 and C26 fatty acids were successfully detected among the metabolic products of C22 and C26 alkanes (Figs. 3(d) and (e)). This directly supports the presence of a classical terminal oxidation pathway in strain SDH15. In contrast, despite cellular growth, no detectable C30 fatty acids were observed during C30 alkane degradation (Fig. 3(f)). This finding suggests that the C30 fatty acid is consumed by the downstream β-oxidation pathway as rapidly as it is formed, preventing its accumulation to detectable levels. This phenomenon reflects a highly efficient and tightly regulated metabolic flux.

Further analyses of complex hydrocarbon mixtures revealed that strain SDH15 produced diverse intermediate fatty acids during degradation. In light paraffin (C10–C24), ESI–MS detected a series of fatty acids ranging from C12 to C23 acids (Fig. 3(g) and Fig. S6 in Appendix A). More importantly, in heavy paraffin (C12–C40), the strain not only generated conventional fatty acids (C12–C27 acids) but also, for the first time, produced ULCFAs up to C56 fatty acid (e.g., C53, C55, C56 acids) (Fig. 3(h) and Fig. S7 in Appendix A).

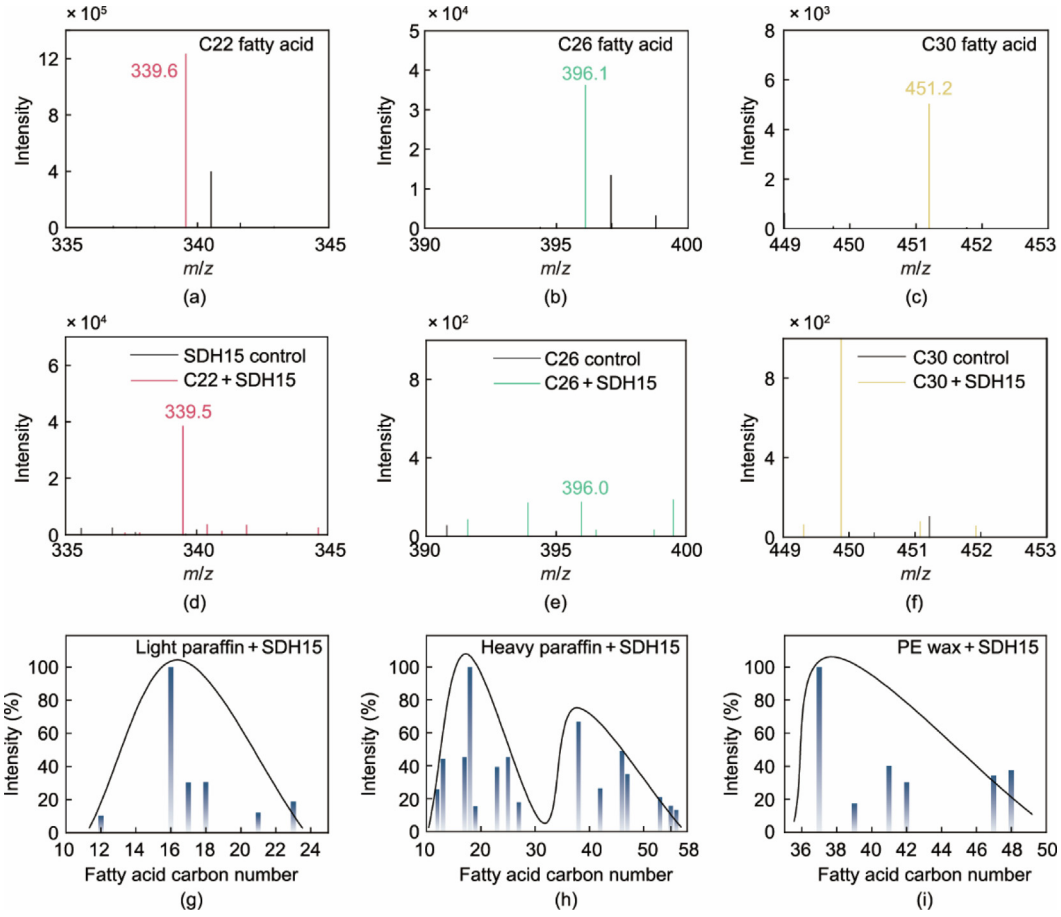

Fig. 3. ESI–MS analysis of fatty acid intermediates produced from long-chain alkane degradation by strain SDH15. (a–c) ESI–MS spectra of fatty acid standards: (a) C22 acid, (b) C26 acid, and (c) C30 acid. (d–f) ESI–MS spectra of degradation products from: (d) C22, (e) C26, and (f) C30. (g–i) Carbon number distribution of fatty acids detected in the degradation products of: (g) light liquid paraffin, (h) heavy liquid paraffin, and (i) PE wax.

This discovery provides strong metabolic evidence for the presence of trace ULCAs beyond C40 in commercial heavy paraffin, while unequivocally demonstrating the upper limit of strain SDH15's oxidative capacity extends to C56. The fatty acid profile exhibited a bimodal distribution with a "detection gap" between C30 and C36. We suggest that for substrates < C30, the rate of fatty acid production outpaces consumption, leading to accumulation. In the C30–C36 range, the two rates become comparable, resulting a potential dynamic balance. For substrates > C36, the consumption of these fatty acids likely becomes the new rate-limiting step, causing the fatty acids to accumulate once more.

Finally, degradation of PE wax further confirmed strain SDH15's exceptional metabolic capability for ULCAs. The detected products included ULCFAs ranging from C37 to C48 fatty acids (Fig. 3(i) and Fig. S8 in Appendix A), consistent with the degradation patterns of components below C56 within the PE wax.

The application of ESI–MS significantly extended the analytical range of conventional GC–MS for identifying long-chain fatty acids, enabling the detection of ultra-long-chain intermediates. Overall, these findings demonstrate that strain SDH15 possesses an unprecedented capacity for the biodegradation of ULCAs, underscoring its promising potential for biotechnological and environmental applications.

3.4. Global functional responses and adaptive mechanisms of strain SDH15

To elucidate the enzymatic mechanisms of ULCAs degradation, we performed a comparative transcriptomic analysis (Fig. S9 in Appendix A). The carbon sources were selected to compare the cellular response between a readily utilized solid substrate and a more recalcitrant one. C22 was chosen as the baseline, as it represents the first *n*-alkane in the series to be solid at the 37 °C incubation temperature. C30 was selected as the representative longer-chain substrate because it presents a greater metabolic challenge while still allowing for a high degree of experimental reproducibility. Although the strain can utilize even longer alkanes such as C40, C30 provides a more suitable balance for generating a high-quality transcriptomic dataset reflective of metabolic adaptation. Sodium acetate was used as a non-alkane control.

A total of 27 185 330–31 773 296 clean reads were obtained from the three parallel samples, with genomic coverage ranging from 98.46% to 99.12% (Table S3 in Appendix A). Correlation analysis indicated that parallel samples showed a strong linear relationship (Fig. S10 in Appendix A), indicating that the transcriptomic sequencing was of a high quality. By examining the differentially expressed genes (DEGs) common to both the C22 and C30 treatments, we characterized the intrinsic multi-enzyme system employed by strain SDH15 for ULCAs degradation. A total of 622 genes exhibited significant differential expression (Figs. 4(a)–(c)). Functional enrichment analysis revealed that upregulated genes were primarily associated with "cell motility" and "lipid transport and metabolism", whereas downregulated genes were enriched in "translation" and "ribosome biogenesis", indicating a strategic reallocation of cellular resources toward alkane metabolism (Fig. S11 in Appendix A).

Among the most strongly expressed genes under alkane conditions were *alkMa* and the fimbrial assembly genes *fimF* and *fimG*

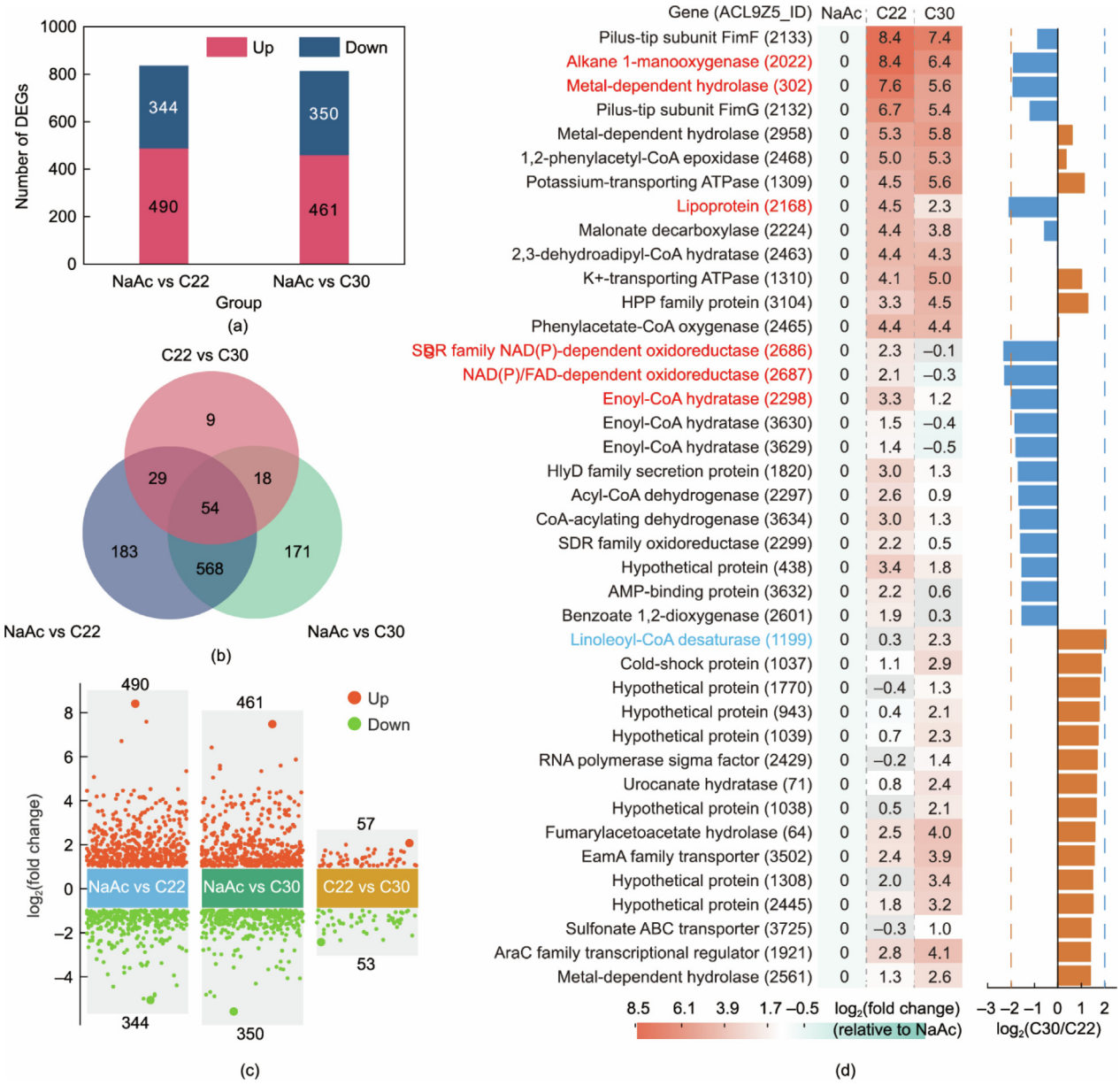

Fig. 4. Transcriptomic analysis of ULCAs metabolism in strain SDH15 under C22 and C30 compared to sodium acetate. (a) Number of DEGs. (b) Venn diagram of DEGs. (c) Multiple differential scatter plots. (d) Heatmap showing the relative abundance of 40 genes, and bar charts showing gene fold changes under C22 and C30. The top 5 genes with the highest expression abundance in the heatmap are marked in bold. In the bar chart, genes with strong upregulation under C22 (log_2(C30/C22) ≤ −2) are marked in blue, and genes with strong upregulation under C30 (log_2(C30/C22) ≥ 2) are marked in red. In panels (d), color intensity represents the log_2(fold change) for statistically significant changes (padj < 0.05); non-significant changes are shown in gray. Hpp: histidine-proline-proline; SDR: short-chain dehydrogenase/reductase; ATPase: adenosine 5'-triphosphatase; NAD(P): nicotinamide adenine dinucleotide (phosphate); FAD: flavin adenine dinucleotide; HlyD: hemolysin D; AMP: adenosine monophosphate; AraC: arabinose C; DEG: differentially expressed gene; NaAc: sodium acetate; K+: potassium.

(Fig. 4(d), Table S4 in Appendix A). The pronounced overexpression of *fimF/G* (up to 332-fold) suggests structural remodeling of cell surface fimbriae to enhance hydrophobic interactions. This interpretation is visually supported by TEM presented below (Fig. 4(f)). Another highly induced gene encoded a metal-dependent hydrolase, predicted to be an R2-type ligand-binding oxidase (Fig. S12 in Appendix A), possibly involved in fatty acid intermediate binding (Fig. 4(d)). Comparison of transcriptional responses revealed chain length-dependent regulatory control in strain SDH15's alkane metabolism (Fig. 4(d)). Genes related to β-oxidation were more highly expressed under C22. Conversely, linoleoyl-coenzyme A (CoA) desaturase (ACL9Z5_1199) was significantly upregulated (4.8-fold) under C30, a change that may directly affect membrane fluidity in response to the longer-chain C30 substrate [40].

3.5. Analysis of strain SDH15's native multi-enzyme system for ULCA degradation

Based on the above differential gene expression analysis, we revealed a highly coordinated multi-enzyme system composed of four functional modules. These modules include chemotaxis and adsorption, transmembrane transport, oxidative degradation, and energy metabolism.

3.5.1. Chemotaxis and adsorption module

Strain SDH15 captures solid alkanes through a two-step "chemotactic sensing-physical adsorption" strategy, which constitutes the critical initial step of the degradation cascade. The chemotaxis gene cluster of strain SDH15 is highly similar to that of *A. dieselolei* (Fig. S13 in Appendix A). Transcriptomic data indicated that, under alkane induction, genes associated with chemotaxis and type IV fimbriae (T4P) biosynthesis were significantly upregulated (1.4–18.8-fold) (Figs. 5(a) and (b), Table S5 in Appendix A). Notably, the core components of the PilH-Chp chemosensory system (*pilH*, *pilG*, *pilI*, *pilJ*, and *chpA*) were activated, suggesting that strain SDH15 can actively sense and orient toward solid ULCAs. During degradation, strain SDH15 adopts a direct contact strategy rather than emulsification mediated by biosurfactants, as evidenced by its high cell surface hydrophobicity (> 90%) and low emulsification index (< 10%) (Fig. 5(c)).

3.5.2. Transmembrane transport module

Adsorbed alkane molecules must traverse the cell envelope to enter the cytoplasm. Transcriptome analysis revealed significant upregulation (1.6- to 2.5-fold) of the genes encoding key outer membrane proteins, including the long-chain fatty acid transporter *fadL*, *ompW*, and *tonB*-dependent receptors (Figs. 6(d) and (e), Table S6 in Appendix A). In the inner membrane, genes encoding members of the major facilitator superfamily (MFS) and the EmrAB-TolC multidrug efflux system (*emrAB-tolC*) were also strongly upregulated (up to 18.9-fold), indicating potential roles in enhancing cellular adaptability and alkane uptake. Transmission electron microscopy confirmed the presence of alkane inclusions within the periplasm and cytoplasm of cells cultured in C22 medium, but not in acetate-grown controls (Fig. 5(f) and Fig. S14 in Appendix A). This directly demonstrates successful intracellular transport of ULCAs.

3.5.3. Oxidative degradation module

Once internalized, alkane molecules are processed by the oxidative degradation module (Fig. 6(a)). At its core lies the AlkB-type alkane monooxygenase AlkMa (ACL9Z5_2022), a specific member of the large AlkB protein family, whose transcript levels increased by 327.7- and 83.8-fold under C22 and C30 conditions, respectively (Fig. 6(b), Table S7 in Appendix A). In contrast, the rubredoxin gene *rubA* (ORF_2821) and rubredoxin reductase gene *rubB* (ORF_2822), which are involved in electron transfer, did not show differential expression on C22 or C30, indicating that these genes are constitutively expressed [41]. Concurrent upregulation of its regulatory factor *alkRa* suggests substrate-induced transcriptional regulation. AlkMa plays a dominant role in the terminal oxidation of ULCAs (C22–C56). In addition, other potential alkane oxidase genes such

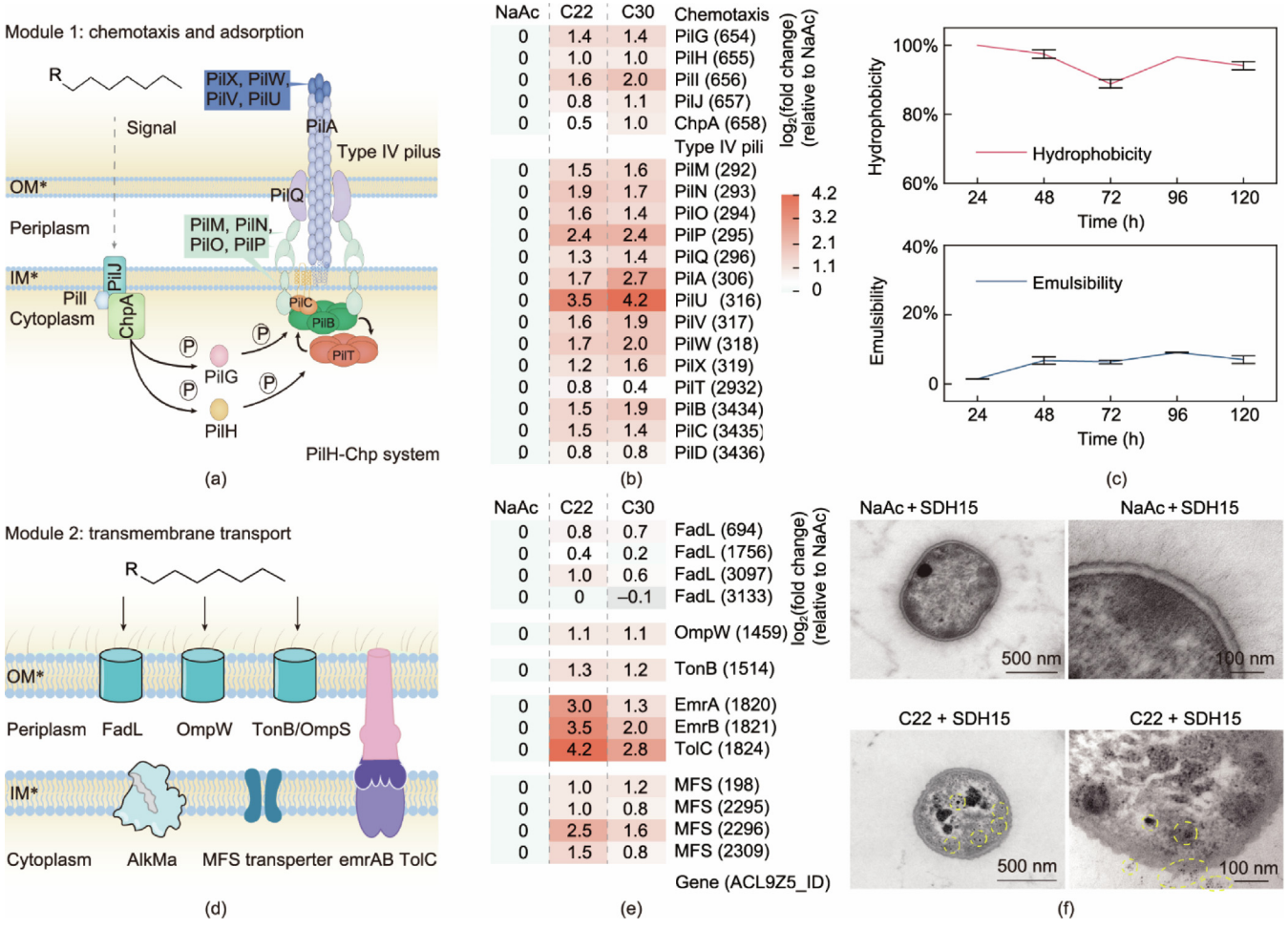

Fig. 5. Chemotaxis, adsorption, and transmembrane transport modules of strain SDH15 for ULCAs utilization. (a) Schematic diagram of the PilH-Chp chemosensory system. (b) Relative expression levels of genes in the PilH-Chp chemosensory system. (c) Cell surface hydrophobicity and emulsification index of strain SDH15 during the degradation of 500 mg·L^{-1} C22. (d) Schematic diagram of the transmembrane transport system. (e) Relative expression levels of genes in the transmembrane transport system. (f) TEM images of strain SDH15 cultured with 500 mg·L^{-1} sodium acetate or C22 as the sole carbon source for 3 days. Yellow circles indicate the presence of C22. In panels (b) and (e), color intensity represents the log$_2$(fold change) for statistically significant changes (padj < 0.05); non-significant changes are shown in gray. MFS: major facilitator superfamily; OM*: outer membrane; IM*: inner membrane.

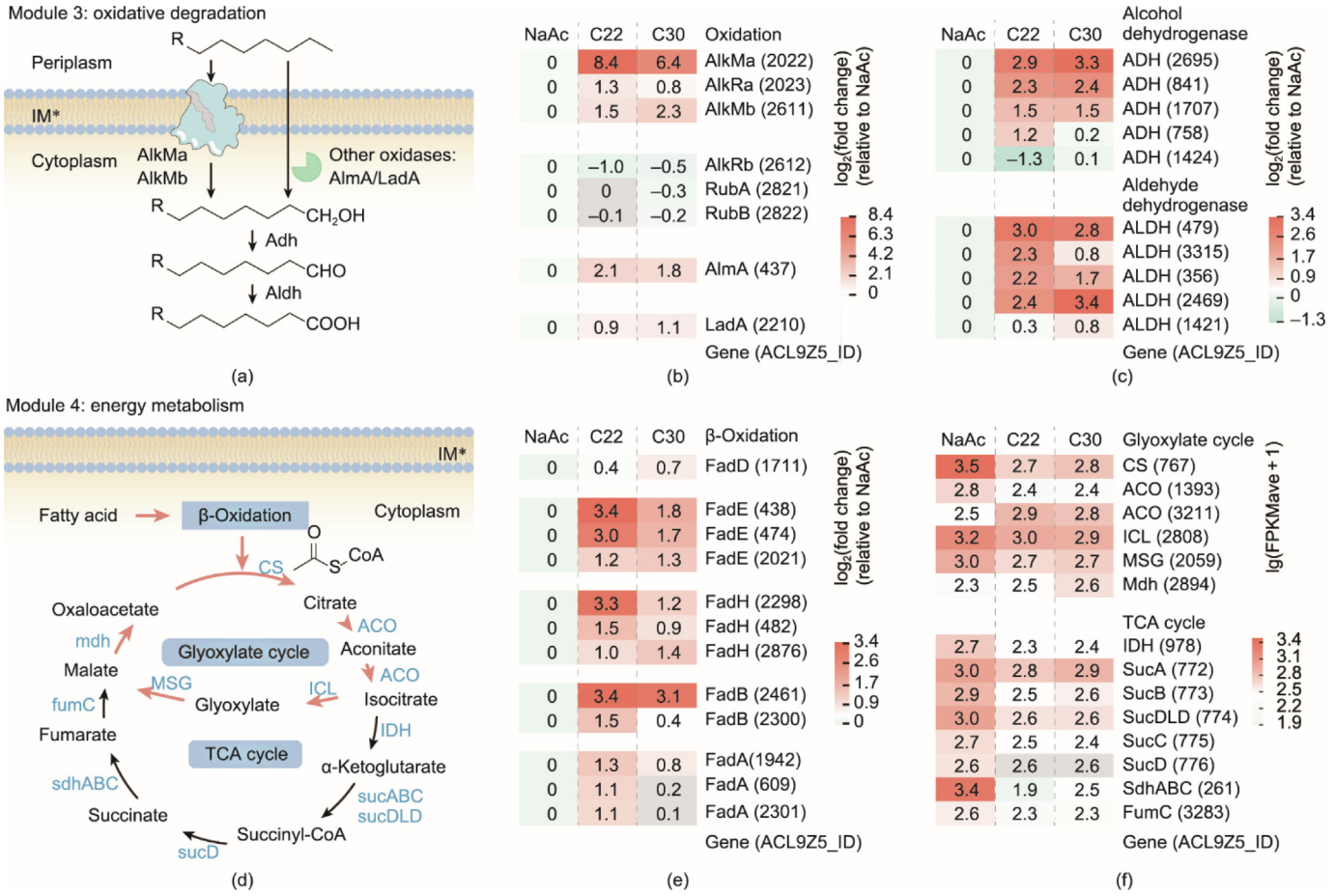

Fig. 6. Oxidative degradation and energy metabolism modules of strain SDH15 for ULCAs utilization. (a) Schematic diagram of the core pathway for ULCAs degradation. (b) Relative expression levels of genes in the initial oxidation pathway. (c) Relative expression levels of genes encoding ADH and ALDH. (d) Schematic diagram of the tricarboxylic acid (TCA) cycle and the glyoxylate cycle. (e) Relative expression levels of genes in the β-oxidation pathway. (f) Relative expression levels of genes in the TCA and glyoxylate cycles. In panels (b), (c), (e), and (f), color intensity represents the $\log_2$(fold change) for statistically significant changes (padj < 0.05); non-significant changes are shown in gray. ICL: isocitrate lyase; CS: citrate synthase; IDH: isocitrate dehydrogenase; ACO: aconitase; MSG: malate synthase G; Mdh: malate dehydrogenase; IM*: inner membrane.

as *alkMb* (ACL9Z5_2611) and *almA* (ACL9Z5_437) were also moderately upregulated (2.9- to 5.1-fold), suggesting they may act synergistically to broaden the substrate range (Fig. S15 in Appendix A). The minor upregulation of *ladA* gene (ACL9Z5_2210, ~2-fold) is consistent with recent studies questioning its function as a primary alkane hydroxylase, which further solidifies the central role of the highly-induced *alkMa* gene in the initial oxidation of ULCAs in strain SDH15.

Following the initial hydroxylation, long-chain alcohols and aldehydes are sequentially oxidized to fatty acids by ADH and ALDH. Phylogenetic trees were constructed by clustering all annotated ADHs and ALDHs from strain SDH15, respectively (Figs. S16 and S17 in Appendix A). Integrative genomic and transcriptomic analyses identified two metal-dependent ADHs (ACL9Z5_1424) and one ALDH (ACL9Z5_1421) as key candidate enzymes (Fig. 6(c), Tables S8 and S9 in Appendix A). To provide direct evidence for their proposed roles, these candidate enzymes were functionally expressed and their catalytic activities were validated through whole-cell biocatalysis, as detailed in Section 3.6.

3.5.4. Energy metabolism module

The resulting fatty acids rapidly enter the β-oxidation pathway, generating acetyl-CoA (Fig. 6(d)). From the transcriptomic data, it was observed that genes encoding enzymes related to β-oxidation were upregulated in expression under C22 and C30 (Fig. 6(e), Table S10 in Appendix A). Transcriptomic evidence indicates that strain SDH15 undergoes metabolic remodeling under alkane-utilizing conditions. This involves partial inhibition of the tricarboxylic acid (TCA) cycle accompanied by upregulation of the glyoxylate shunt genes encoding isocitrate lyase (ICL) and malate synthase (MSG) (Fig. 6(f), Table S11 in Appendix A). This adaptive strategy bypasses TCA decarboxylation, thereby conserving carbon skeletons for biosynthesis. The energy metabolism module thus supplies adenosine 5'-triphosphate (ATP) and reducing power for energetically demanding upstream processes, including chemotaxis, transport, and oxidation, enabling robust growth on solid ULCAs.

3.6. Functional verification of the core oxidative degradation module

To elucidate the physiological role of AlkMa in ULCAs degradation, an *alkMa*-deficient mutant (SDH15Δ*alkMa*) was constructed and evaluated for growth and degradation efficiency using C22–C40 alkanes as sole carbon sources. Compared to the wild-type strain, the mutant exhibited significantly impaired growth on C22, C26, and C30, with the inhibitory effect being most pronounced on C22. Regarding degradation efficiency, the most substantial decrease was observed for C30, where the rate dropped from 20.3% to 5.6%. These results confirm that AlkMa is essential for the utilization of alkanes within this range (Figs. 7(a) and (b)). However, the mutant's growth and degradation capacity were not completely abolished. This suggests that the presence and

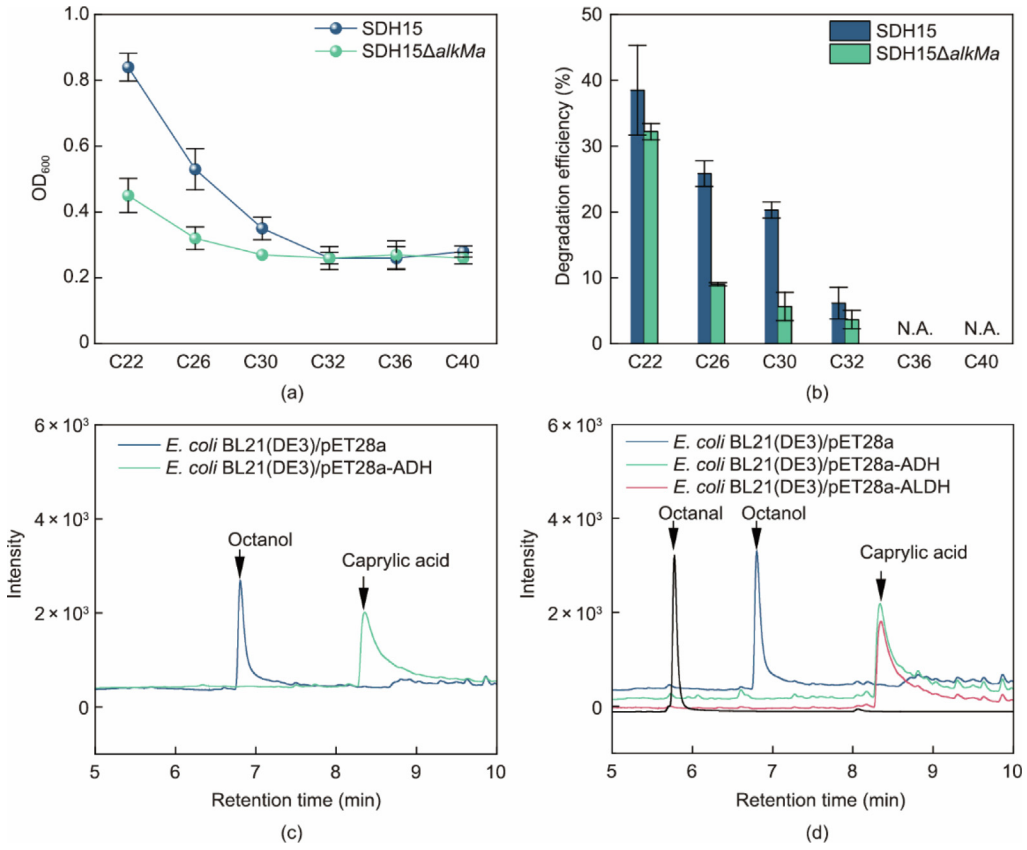

Fig. 7. Functional verification of enzymes in the oxidative degradation module. (a, b) Comparison of wild-type and Δ*alkMa* mutant strains based on (a) cell density (OD_{600}) and (b) degradation efficiency after 5 days of culture on *n*-alkanes (C22–C40). Data are mean ± SD (n = 3). (c, d) Gas chromatograms from whole-cell biocatalysis assays using recombinant *E. coli*. (c) Activity of the ADH strain on 1-octanol. (d) Activity of the ADH and ALDH strains on 1-octanal. The control in both panels was *E. coli* with an empty vector; N.A.: not applicable.

activity of other compensatory alkane hydroxylases in strain SDH15, which can compensate for the loss of AlkMa. No significant differences were observed between the mutant and wild-type strains on longer alkanes (C32, C36, and C40). It is possible that for these very long solid alkanes, the overall degradation rate is co-limited by physical factors, such as substrate bioavailability [38], which may mask the full impact of the *alkMa* deletion.

To functionally validate the candidate dehydrogenases, whole-cell biocatalysis assays were performed using recombinant *E. coli*. The candidate *adh* gene (ACL9Z5_1424) demonstrated potent bifunctional activity, completely converting 1-octanol to the final product, octanoic acid, without any detectable accumulation of the aldehyde intermediate (Figs. 7(c) and (d)). The *aldh* gene (ACL9Z5_1421) was confirmed to be an ALDH, effectively oxidizing octanal to octanoic acid (Fig. 7(d)). The empty-vector control strain displayed an endogenous reductase activity, converting octanal back to 1-octanol. The oxidative performance of the recombinant ALDH strain, despite this competing host reaction, confirms its catalytic function. Collectively, these functional assays provide direct evidence that they play critical roles in the post-hydroxylation steps of the oxidative degradation module in strain SDH15.

3.7. An integrated model for ULCAs biodegradation in strain SDH15

By integrating multi-omics methods, such as genomics and transcriptomics, we propose a comprehensive model describing how strain SDH15 achieves the biodegradation of solid ULCAs up to C56 (Fig. 8). The process operates through four tightly coordinated modules.

The degradation cascade begins with active environmental sensing and substrate capture. The PilH-Chp chemosensory system detects solid alkanes, guiding T4P-driven motility. Overexpressed of the genes encoding usher proteins FimF/G reinforce pili structure, promoting efficient adsorption of hydrophobic substrates. Once attached, outer membrane proteins (FadL, OmpW, and TonB) and inner membrane MFS transporters cooperate to import alkane molecules into the cytoplasm, forming observable intracellular inclusions.

Intracellularly, the oxidation module initiates catalysis. The highly upregulated *alkMa* gene encodes the monooxygenase AlkMa, which catalyzes terminal oxidation of alkanes, initiating conversion to fatty alcohols, which are further oxidized by ADH and ALDH to fatty acids. These intermediates subsequently enter the β-oxidation and glyoxylate cycles, yielding ATP and biosynthetic precursors. This metabolic network fuels both cellular growth and energy-demanding upstream functions, from motility to enzyme biosynthesis.

However, the ultimate fate of these ULCFA intermediates may be influenced by the chain-length limits of the downstream catabolic pathway, particularly the initial activation step by acyl-CoA synthetases [42]. The ability of SDH15 to grow on C40 as a sole carbon source suggests the presence of a catabolic system with an exceptionally broad substrate range. For even longer chains like C56, it is plausible that a catabolic threshold exists, beyond which these intermediates might be produced but no longer efficiently degraded. Therefore, the final products could be chain-length dependent, potentially resulting in complete mineralization to CO_2, shortening for incorporation into membrane lipids [43], or

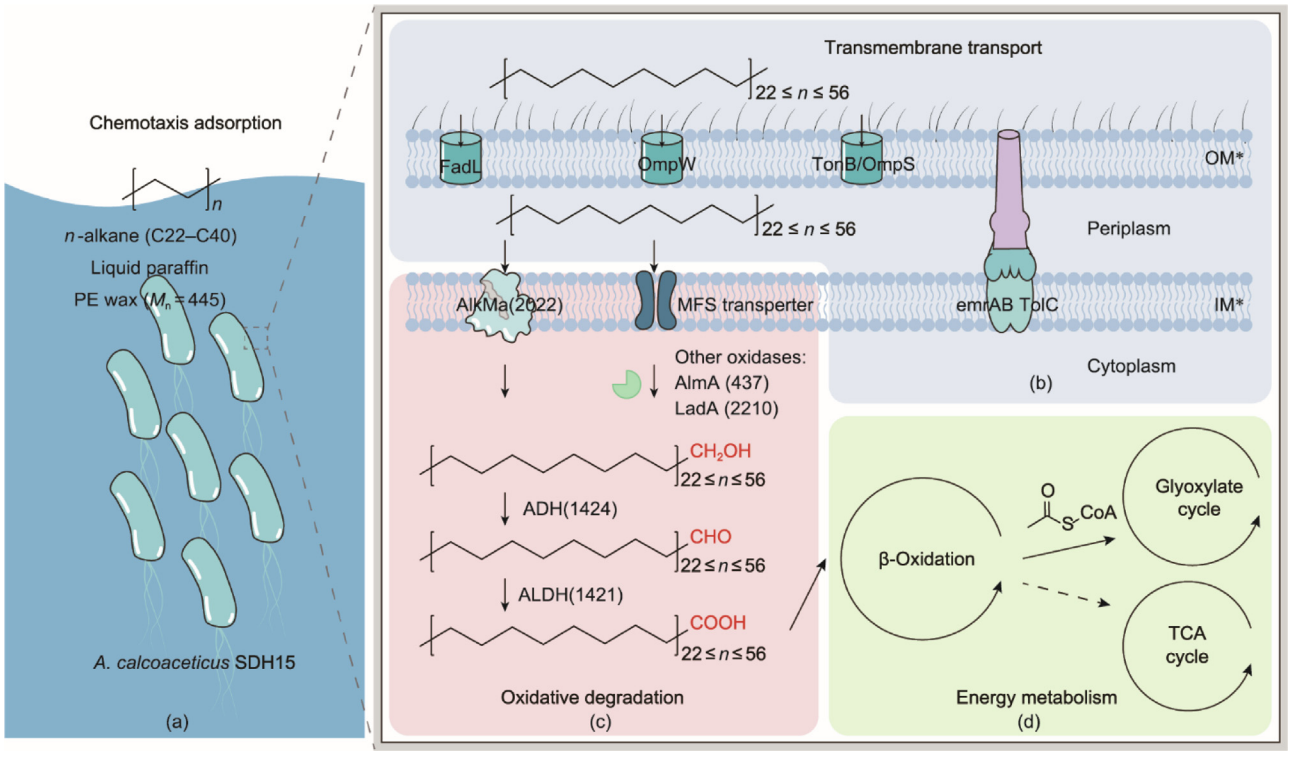

Fig. 8. Key pathway of ULCAs degradation by strain SDH15. This diagram illustrates four tightly coordinated modules: (a) Chemotaxis and adsorption: Driven by PilH-Chp signaling and reinforced Type IV pili (*fimF*/*G* upregulated 332-fold). (b) Transmembrane transport: Involving outer membrane proteins FadL, OmpW, and TonB (*fadL*/*ompW*/*tonB* upregulated 1.6- to 2.5-fold) and inner membrane MFS/EmrAB-TolC systems (*mfs*/*emrAB-tolC* up to 18.9-fold). (c) Oxidative degradation: Initiated by the essential AlkMa monooxygenase (*alkMa* upregulated 327-fold for C22) and followed by ADH/ALDH. (d) Energy metabolism: Featuring β-oxidation and an adaptive shift to the glyoxylate cycle (*icl*/*msg* upregulated) for carbon conservation. This tightly integrated system enables the catabolism of alkanes up to C56. M_n: number-average molecular weight.

accumulation of the ULCFA itself if it exceeds the cell's catabolic limit.

In summary, the remarkable catabolic performance of strain SDH15 arises not from a single enzyme but from a sophisticated, multi-module system integrating efficient substrate capture, rapid transport, oxidation, and adaptive energy metabolism. This molecular framework illuminates a natural mechanism for decomposing highly recalcitrant hydrocarbons and provides a foundation for the rational design of synthetic microbial systems for PE bioremediation.

4. Conclusions

This study fundamentally expands the known boundaries of microbial hydrocarbon catabolism by identifying *A. calcoaceticus* SDH15, a novel isolate capable of metabolizing solid ULCAs up to C56. By integrating genomics and transcriptomics, we reveal the native multi-enzyme system of strain SDH15 for degrading ULCAs. The process operates through four synergistic modules: chemotaxis-driven substrate capture, efficient transmembrane transport, potent terminal oxidation catalyzed by the essential monooxygenase AlkMa, and an adaptive metabolic shift to the glyoxylate cycle for carbon conservation. The direct detection of a C56 fatty acid intermediate provides unequivocal molecular proof of the pathway's exceptional breadth. These findings establish a robust foundation for the rational design of next-generation synthetic microbes. Future work should express and optimize the cascade in an industrial host, enhance electron transfer to the monooxygenase, and tune regulators to respond to PE oligomers. Such advances are critical to accelerating the development of scalable biotechnologies that will drive a truly circular plastics economy.

CRediT authorship contribution statement

Xianrui Liu: Writing – original draft, Data curation. **Donghuan Su:** Data curation. **Shaojie Wang:** Writing – review & editing, Funding acquisition, Conceptualization. **Zhenxia Du:** Methodology, Conceptualization. **Haijia Su:** Writing – review & editing, Funding acquisition, Conceptualization.

Data availability

The raw genome and transcriptome sequence reads of *A. calcoaceticus* SDH15 were deposited in the Sequence Read Archive under accession number PRJNA1211330.

Declaration of competing interest

The authors declare that they have no known competing financial interests or personal relationships that could have appeared to influence the work reported in this paper.

Acknowledgment

This work was supported by the National Natural Science Foundation of China (22578021 and 22308018), the Beijing Natural Science Foundation (2252017), and the Fundamental Research Funds for the Central Universities (buctrc202341 and JD2537).

Appendix A. Supplementary material

Supplementary data to this article can be found online at https://doi.org/10.1016/j.eng.2026.02.035.

References

[1] Geyer R, Jambeck JR, Law KL. Production, use, and fate of all plastics ever made. Sci Adv 2017;3(7):e1700782.
[2] Lv H, Huang F, Zhang F. Upcycling waste plastics with a C–C backbone by heterogeneous catalysis. Langmuir 2024;40(10):5077–89.
[3] Faust K, Denifl P, Hapke M. Recent advances in catalytic chemical recycling of polyolefins. ChemCatChem 2023;15(13):e202300310.
[4] Pottinger AS, Geyer R, Biyani N, Martinez CC, Nathan N, Morse MR, et al. Pathways to reduce global plastic waste mismanagement and greenhouse gas emissions by 2050. Science 2024;386(6726):1168–73.
[5] Qian X, Liu J, Xue R, Liu H, Wen X, Yang L, et al. Synthetic biology boosts biological depolymerization and upgrading of waste plastics. Synth Biol J 2021;2(2):161–80.
[6] Salgado-Brito R, Neria MI, Mesta-Howard AM, Díaz Cedillo F, Wang ET. Oxidation of solid paraffin (C11–40) by *Pseudomonas aeruginosa* MGP-1. Ann Microbiol 2007;57(3):321–8.
[7] Oiffer T, Leipold F, Süss P, Breite D, Griebel J, Khurram M, et al. Chemo-enzymatic depolymerization of functionalized low-molecular-weight polyethylene. Angew Chem Int Ed Engl 2024;63(50):e202415012.
[8] Jin J, Arciszewski J, Auclair K, Jia Z. Enzymatic polyethylene biorecycling: confronting challenges and shaping the future. J Hazard Mater 2023;460:132449.
[9] Suzuki M, Hayashi T, Takahashi K, Nozaki K, Kasuya KI. Exploring biodegradation limits of *n*-alkanes as polyethylene models using multi-omics approaches. Sci Total Environ 2025;977:179365.
[10] Throne-Holst M, Markussen S, Winnberg A, Ellingsen TE, Kotlar HK, Zotchev SB. Utilization of *n*-alkanes by a newly isolated strain of *Acinetobacter venetianus*: the role of two AlkB-type alkane hydroxylases. Appl Microbiol Biotechnol 2006;72(2):353–60.
[11] Sakai Y, Maeng JH, Tani Y, Kato N. Use of Long-chain *n*-alkanes (C_{13}–C_{44}) by an Isolate, *Acinetobacter* sp. M-1. Biosci Biotechnol Biochem 1994;58(11):2128–30.
[12] Haines JR, Alexander M. Microbial degradation of high-molecular-weight alkanes. Appl Microbiol 1974;28(6):1084–5.
[13] Liu F, Zhang N, Shang Y, Yao M, Ding M, Yuan Y. Construction of *Yarrowia lipolytica* for degradation of low-density polyethylene. Process Saf Environ Prot 2025;195:106818.
[14] Bai F, Fan J, Zhang X, Wang X, Liu S. Biodegradation of polyethylene with polyethylene-group-degrading enzyme delivered by the engineered *Bacillus velezensis*. J Hazard Mater 2025;488:137330.
[15] Tang Z, Zhao Y, Wang Z, Liu X, Liu Y, Gu P, et al. Cobalt catalyzed carbonyl functionalization to boost the biodegradation of polyethylene by *Bacillus velezensis* C5. Chem Eng J 2024;495:153226.
[16] Wentzel A, Ellingsen TE, Kotlar HK, Zotchev SB, Throne-Holst M. Bacterial metabolism of long-chain *n*-alkanes. Appl Microbiol Biotechnol 2007;76 (6):1209–21.
[17] Kurata S, Yamaguchi K, Nagai M. Rapid discrimination of fatty acid composition in fats and oils by electrospray ionization mass spectrometry. Anal Sci 2005;21(12):1457–65.
[18] Rydlewski AA, Manin LP, Pizzo JS, Silva PD, da Silveira R, Tavares CBG, et al. Lipid profile by direct infusion ESI–MS and fatty acid composition by GC-FID in human milk: association with nutritional status of donors. J Food Compos Anal 2021;100:103797.
[19] Řezanka T, Sigler K. Identification of very long chain fatty acids from sugar cane wax by atmospheric pressure chemical ionization liquid chromatography-mass spectroscopy. Phytochemistry 2006;67(9):916–23.
[20] Fenibo EO, Selvarajan R, Abia ALK, Matambo T. Medium-chain alkane biodegradation and its link to some unifying attributes of *alkB* genes diversity. Sci Total Environ 2023;877:162951.
[21] Liu J, Zhao B, Lan Y, Ma T. Enhanced degradation of different crude oils by defined engineered consortia of *Acinetobacter venetianus* RAG-1 mutants based on their alkane metabolism. Bioresour Technol 2021;327:124787.
[22] Chen S, Liu J, Gao G, Li M, Cao L, Liu T, et al. An NAD^+-dependent group III alcohol dehydrogenase involved in long-chain alkane degradation in *Acinetobacter venetianus* RAG-1. Enzyme Microb Technol 2024;172:110343.
[23] Park C, Shin B, Jung J, Lee Y, Park W. Metabolic and stress responses of *Acinetobacter oleivorans* DR1 during long-chain alkane degradation. Microb Biotechnol 2017;10(6):1809–23.
[24] Feng L, Wang W, Cheng J, Ren Y, Zhao G, Gao C, et al. Genome and proteome of long-chain alkane degrading *Geobacillus thermodenitrificans* NG80-2 isolated from a deep-subsurface oil reservoir. Proc Natl Acad Sci USA 2007;104 (13):5602–7.
[25] Mireles R, Matthews A, Teufel R, Noda-García L. Can flavoprotein monooxygenases functionalize long-chain *n*-alkanes? PLoS One 2025;20(9): e0332702.
[26] Yin CF, Nie Y, Li T, Zhou NY. AlmA involved in the long-chain *n*-alkane degradation pathway in *Acinetobacter baylyi* ADP1 is a Baeyer–Villiger monooxygenase. Appl Environ Microbiol 2024;90(1):e01625–e1723.
[27] Wang W, Shao Z. The long-chain alkane metabolism network of *Alcanivorax dieselolei*. Nat Commun 2014;5(1):5755.
[28] Kothari A, Charrier M, Wu YW, Malfatti S, Zhou CE, Singer SW, et al. Transcriptomic analysis of the highly efficient oil-degrading bacterium *Acinetobacter venetianus* RAG-1 reveals genes important in dodecane uptake and utilization. FEMS Microbiol Lett 2016;363(20):fnw224.
[29] Liu J, Chen S, Zhao B, Li G, Ma T. A novel FadL homolog, AltL, mediates transport of long-chain alkanes and fatty acids in *Acinetobacter venetianus* RAG-1. Appl Environ Microbiol 2022;88(20):e01294–322.
[30] Xu HX, Tang YQ, Nie Y, Wu XL. Comparative transcriptome analysis reveals different adaptation mechanisms for degradation of very long-chain and normal long-chain alkanes in *Dietzia* sp. DQ12-45-1b. Environ Microbiol 2022;24(4):1932–45.
[31] Liu X, Zhang Y, Sun Q, Liu Z, Zhao Y, Fan A, et al. Rapid colonization and biodegradation of untreated commercial polyethylene wrap by a new strain of *Bacillus velezensis* C5. J Environ Manage 2022;301:113848.
[32] Folch J, Lees M, Stanley GHS. A simple method for the isolation and purification of total lipides from animal tissues. J Biol Chem 1957;226(1): 497–509.
[33] Liu Y, Wu J, Liu Y, Wu X. Biological process of alkane degradation by *Gordonia sihwaniensis*. ACS Omega 2022;7(1):55–63.
[34] Rosenberg M, Gutnick D, Rosenberg E. Adherence of bacteria to hydrocarbons: a simple method for measuring cell-surface hydrophobicity. FEMS Microbiol Lett 1980;9(1):29–33.
[35] Dong Y, Yan J, Du H, Chen M, Ma T, Feng L. Engineering of LadA for enhanced hexadecane oxidation using random- and site-directed mutagenesis. Appl Microbiol Biotechnol 2012;94(4):1019–29.
[36] Ishige T, Tani A, Sakai Y, Kato N. Long-chain aldehyde dehydrogenase that participates in *n*-alkane utilization and wax ester synthesis in *Acinetobacter* sp. strain M-1. Appl Environ Microbiol 2000;66(8):3481–6.
[37] Rojo F. Degradation of alkanes by bacteria. Environ Microbiol 2009;11 (10):2477–90.
[38] Marghade DT, Chahande AD, Tiwari MS, Patil PD. Microbial Degradation of Xenobiotic Compounds. In: Inamuddin Ahamed MI, Prasad R, editors. Recent advances in microbial degradation. Berlin: Springer; 2021. p. 173–217.
[39] Chen J, Nichols KK, Wilson L, Barnes S, Nichols JJ. Untargeted lipidomic analysis of human tears: a new approach for quantification of *O*-acyl-omega hydroxy fatty acids. Ocul Surf 2019;17(2):347–55.
[40] Cybulski LE, Albanesi D, Mansilla MC, Altabe S, Aguilar PS, de Mendoza D. Mechanism of membrane fluidity optimization: isothermal control of the Bacillus subtilis acyl-lipid desaturase. Mol Microbiol 2002;45(5): 1379–88.
[41] Tani A, Ishige T, Sakai Y, Kato N. Gene structures and regulation of the alkane hydroxylase complex in *Acinetobacter* sp. strain M-1. J Bacteriol 2001;183 (5):1819–23.
[42] Andersson CS, Lundgren CAK, Magnúsdóttir A, Ge C, Wieslander A, Molina DM, et al. The *Mycobacterium tuberculosis* very-long-chain fatty acyl-CoA synthetase: structural basis for housing lipid substrates longer than the enzyme. Structure 2012;20(6):1062–70.
[43] Radka CD, Frank MW, Rock CO, Yao J. Fatty acid activation and utilization by *Alistipes finegoldii*, a representative Bacteroidetes resident of the human gut microbiome. Mol Microbiol 2020;113(4):807–25.